

Free boundary value problems associated with the growth and development of multicellular spheroids

H. M. BYRNE¹ and M. A. J. CHAPLAIN²

¹*Department of Mathematics, UMIST, PO Box 88, Manchester M60 1QD, UK (email:h.byrne@umist.ac.uk)*

²*Department of Mathematics and Computer Science, University of Dundee, Dundee DD1 4HN, UK
(email: Chaplain@mcs.dundee.ac.uk)*

(Received 30 August 1996; received in revised form 5 March 1997)

In this paper a generalized model for the growth of avascular tumours is presented. The formulation leads naturally to the incorporation of free boundaries which define the outer tumour surface explicitly and various inner surfaces implicitly. A combination of numerical simulations, asymptotic analysis and perturbation techniques is used to study the model and yields results, which agree well with experimentally-observed phenomena.

1 Introduction

Over the past 20 years, advances in the theory of free boundary value problems have been stimulated by the marked increase in the number of mathematical models used to describe actual physical problems [1–4]. More recently, mathematical biology is proving to be a rich source of similar free boundary value problems [5]. Of particular interest in this paper is a class of free and moving boundary value problems which have been proposed to describe the growth of multicellular spheroids (MCS). MCS are clusters of cancer cells, used in the laboratory to study the early stages of avascular tumour growth. Mature MCS possess a well-defined structure, comprising a central core of necrotic, or dead, cells, surrounded by a layer of non-proliferating, quiescent cells, with proliferating cells restricted to the outer, nutrient-rich layer of the tumour [6–10]. As such, they are often used to assess the efficacy of new anti-cancer drugs and treatment therapies.

Progress in modelling tumour growth has been largely guided by experimental results. Thus, the majority of mathematical models focus on the growth of MCS or avascular tumour growth. However, several models have been proposed to describe angiogenesis [11–16]. This process marks the transition from the relatively harmless, and localized, avascular state described above, to the more dangerous vascular state, wherein the tumour possesses the ability to invade surrounding tissue and metastasize to distant parts of the body. Angiogenesis is the process by which tumours induce blood vessels from the host tissue to sprout capillary tips which migrate towards and ultimately penetrate the tumour, providing it with a circulating blood supply and, therefore, an almost limitless source of nutrients [17–19]. The vascular growth phase which follows angiogenesis is marked by a rapid increase in cell proliferation, and is usually accompanied by an increase in the pressure at the centre of the tumour. This may be sufficient to occlude blood vessels and, thereby, to restrict drug delivery to the tumour [20, 21]. Apart from several papers which focus on the invasive potential of tumours [22–25], to date, modelling of this vascular phase has been largely overlooked.

In this paper we focus on the evolution of a MCS growing in response to a single, externally-supplied nutrient, such as oxygen or glucose, and two growth inhibitors. We assume that the tumour adopts a multi-layered structure, with proliferating cells in the outer shell, quiescent cells in the middle shell, and necrotic cells in the central core. The proportion of each cell type changes as the tumour grows. Consider, for example, the growth of a tumour that initially comprises only proliferating cells. As the tumour grows, cells towards its centre, being deprived of vital nutrients, cease proliferating and become quiescent. (Quiescent cells are not dead: they simply do not divide. If the environmental conditions improve, i.e. nutrient levels increase, then such cells may recommence proliferating. Thus quiescence is a reversible state.) Further growth of the tumour is accompanied by an increase in the quiescent cell population and a reduction in the minimum nutrient concentration, until eventually cells towards the centre of the tumour, being starved of vital nutrients, become necrotic.

Mathematical models of MCS typically consist of an ordinary differential equation (ODE) coupled to at least one Reaction-Diffusion Equation (RDE) [14, 26–34]. The ODE derives from mass conservation and describes the evolution of the outer tumour boundary, whereas the RDEs describe the distribution within the tumour of vital nutrients, such as oxygen and glucose, and growth inhibitors. Such models accurately reproduce the growth of spheroids and the macroscopic heterogeneity which is the hallmark of spheroids. Whilst the model developed in this paper also exhibits these features, the approach adopted gives rise to a more generic description of tumour growth than has been evident in earlier work. In particular, we show how previous models can be recovered as special cases of our generic model. A further consequence of our approach is that we are able to generate a number of experimentally verifiable hypotheses. For example, our analysis suggests that immediately after the onset of quiescence or necrosis the total tumour volume remains approximately constant whilst there is a rapid increase in the volume of the quiescent (or necrotic) cells. We also derive necessary conditions in terms of key physical parameters for obtaining tumours with thin proliferating rims (such structures are frequently observed when MCS are grown *in vitro*). These and other model predictions are discussed in the conclusions.

An important feature of our model formulation is that it enables us to assess a tumour's potential for invasion and to ascribe this ability to physical mechanisms. The key feature that determines this is the balance between an internal expansive force (caused by cell proliferation) and a restraining force (caused by forces of adhesion which exist between cells on the tumour boundary).

The model derivation follows Greenspan [24]: the tumour is treated as an incompressible fluid, with cell death and birth causing local changes in the cell population. These in turn generate pressure gradients which drive cell motion and induce expansion of the tumour. Unlike Greenspan, who assumes that the tumour comprises a large necrotic core and a thin proliferating rim, we make no assumptions about the width of the proliferating rim or the tumour's structure. Arguably, the most striking difference between Greenspan's model and ours is the manner in which surface tension effects are incorporated [22]. Greenspan assumes that, on the surface of the tumour, the surface tension force which maintains the compactness of the MCS balances the internal expansive pressure per unit surface area. Working on an infinite domain he assumes further that the nutrient concentration is continuous across the tumour boundary but that the flux of nutrient is not. In contrast, we

restrict attention to the moving domain defined by the tumour volume and assume that the nutrient concentration satisfies the Gibbs–Thomson relation on the boundary [35, 36]. This relation states that the nutrient concentration at a point on the tumour boundary is less than the external concentration by a factor which is proportional to the local curvature there. This energy is needed by cells on the periphery to preserve the forces of adhesion which exist to maintain the tumour’s compactness. Clear experimental evidence for these effects can be found in Miyasaka [37] and Nagle *et al.* [38], and references therein.

Any interior boundaries, such as the interface between the necrotic core and the quiescent region, are defined implicitly, occurring when the nutrient concentration attains prescribed values. A combination of numerical simulations, asymptotic analysis and perturbation methods can be used to analyse the model. The results presented here build upon and extend results given elsewhere [22, 24, 26, 28, 31, 34]. As such, the paper provides a review of approaches currently being used to model avascular tumour growth.

In vitro observations [8, 9, 39] suggest that in the early stages solid tumours remain approximately spherical as they grow. Therefore, our analysis focuses on the existence and stability of radially-symmetric solutions of the model equations. We show how the pressure can be eliminated from the model when radial symmetry is assumed and how a reduced system of equations which is similar in form to existing models of MCS [26, 27, 31] can be recovered. We believe that our derivation of this simplified model indicates how models of avascular tumour growth arise as special cases of more physically based models.

Perturbation analysis shows how the existence and stability of radially symmetric solutions depends on key parameters, such as the external nutrient concentration and cell-cell adhesion (see Figure 1). As the strength of the cell-cell adhesion bonds increases then the size of the stable steady state solutions decreases until the bonds are so strong that no steady solutions exist. We also investigate how asymmetric perturbations from radial symmetry develop in time. If all asymmetric perturbations ultimately disappear then we conclude that the tumour will simply grow as a radially-symmetric mass. By contrast, the growth of a perturbation implies that the tumour has a propensity for asymmetric local invasion, the growth rate of the perturbation indicating the degree of aggression. Our analysis suggests that as the strength of the cell-cell adhesion bonds increases the number of modes to which the tumour is unstable decreases (see Figure 3). Thus we conclude that accurate measurement of this parameter may prove a useful indicator of a tumour’s propensity for invasion.

2 Model formulation

The mathematical model studied in this paper describes an MCS which contains proliferating, quiescent and necrotic cells. Implicit in the model are a number of assumptions that are routinely adopted by other authors [12, 26, 27, 29–31]. For example, no explicit mention is made of the tumour cells: instead, we assume that the local concentration of an externally-supplied nutrients provides an accurate measure of the cell density and type, with high nutrient levels indicating rapid cell proliferation and low levels indicating cell death due to necrosis. In addition, interactions with the external environment are neglected – this might be the case for a tumour colony grown *in vitro*. Finally, we assume that the tumour maintains a multi-layered configuration as it grows, with proliferating cells restricted to the outer shell, quiescent cells in an adjacent region, and necrotic cells localized at the tumour’s centre.

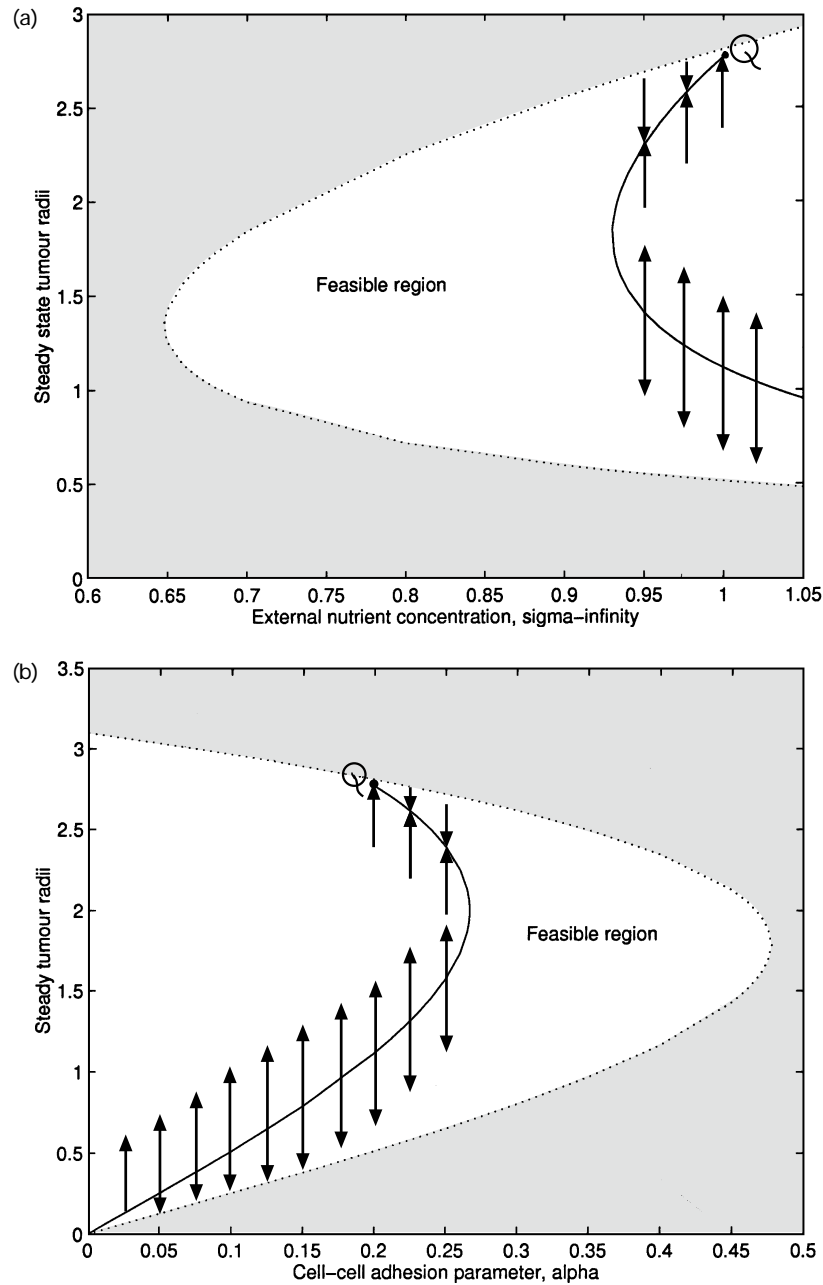


FIGURE 1. (a) Diagram showing how the existence, uniqueness and magnitude of the steady-state tumour radius depend on the external nutrient concentration σ_∞ (solid curve). For small values of σ_∞ ($\sigma_\infty < 0.93$) no steady solutions occur. For larger values of σ_∞ ($0.93 < \sigma_\infty < 1.00$) two non-trivial solutions exist. When $\sigma_\infty > 1.00$ the upper solution becomes quiescent: the point Q marks the onset of quiescence. Where they exist, solutions on the upper branch are stable with respect to time-dependent perturbations whereas solutions on the lower branch are unstable. The dotted curve shows how the range of R for which time-dependent non-quiescent solutions exist varies with σ_∞ (see Eq. (3.3)). For a fixed value of σ_∞ valid non-quiescent solutions exist within the (unshaded) feasible region. Parameter values: $\sigma_\infty = 1.0$, $\tilde{\sigma} = 0.6$, $\sigma_Q = 0.1$, $\lambda_0 = 0.5$, $s = 100.0$. (b) Diagram showing how the steady-state tumour radius varies with the cell-cell adhesion parameter α (solid curve). As in Figure

We focus on the effect that three growth factors have on the tumour's development. These are: (i) an externally-supplied nutrient (σ), such as oxygen or glucose; (ii) an externally-supplied growth-inhibitor (β) which may be regarded as either an anti-cancer drug or a chemical produced *in vivo* as part of the immune response to the tumour; and, (iii) an internally-produced growth-inhibitor (ω) which may be regarded as a bi-product of the degradation of the necrotic cells. RDEs describe the evolution of σ , β and ω , and F_σ , F_β and F_ω denote their respective reaction rates. We remark that a typical chemical diffusion timescale (\sim mins) is much shorter than a typical tumour doubling time (\sim days) [26, 29, 31]. This means that, as the tumour grows, σ , β and ω rapidly redistribute throughout the new volume. By scaling time with the tumour growth timescale we set $\partial/\partial t \equiv 0$ in the RDEs

$$0 = \nabla^2 \sigma + F_\sigma = \nabla^2 \beta + F_\beta = \nabla^2 \omega + F_\omega. \quad (2.1)$$

In (2.1) the (assumed constant) diffusion coefficients have been absorbed into F_σ , F_β and F_ω .

If we regard the tumour as an incompressible fluid, then local changes in the cell population, caused by cell birth and death, will induce motion of neighbouring cells. We denote the proliferation rate at a point inside the tumour by $S = S(\sigma, \beta, \omega)$. Introducing the cell velocity $\mathbf{u}(\mathbf{r}, t)$ (where \mathbf{r} is the position vector in spherical polar coordinates) and applying mass conservation we derive the following equation for \mathbf{u} :

$$\nabla \cdot \mathbf{u} = S(\sigma, \beta, \omega). \quad (2.2)$$

The equation of motion of a point on the outer boundary of the tumour is given by

$$\hat{\mathbf{n}} \cdot \frac{d\mathbf{r}}{dt} = \mathbf{u} \cdot \hat{\mathbf{n}} \quad \text{on } \Gamma(\mathbf{r}, t) = 0, \quad (2.3)$$

where $\hat{\mathbf{n}}$ is an outward unit normal vector and

$$\Gamma(\mathbf{r}, t) = 0 = r - R(\theta, \phi, t).$$

Free-boundaries $\Gamma_Q(\mathbf{r}, t) = 0$ and $\Gamma_N(\mathbf{r}, t) = 0$ are introduced to delineate regions of cell proliferation, quiescence and necrosis:

$$\Gamma_Q(\mathbf{r}, t) = 0 = r - R_Q(\theta, \phi, t) \quad \text{and} \quad \Gamma_N(\mathbf{r}, t) = 0 = r - R_N(\theta, \phi, t).$$

These interfaces are defined implicitly, arising when σ passes through prescribed critical values (cf. Stefan problems, with nutrient concentration analogous to temperature): the quiescent interface occurs when $\sigma = \sigma_Q$ and the necrotic interface when $\sigma = \sigma_N < \sigma_Q$ (see Eqs. (2.9)–(2.10)). Thus, cells cease proliferating, but remain viable, if $\sigma_N < \sigma < \sigma_Q$ and necrosis occurs whenever $\sigma < \sigma_N$.

1(a), the dotted curve shows how the range of R for which time-dependent solutions exist varies with α . The point Q marks the onset of quiescence: for smaller values of α ($\alpha < 0.20$) solutions on the upper branch possess a quiescent region. Parameter values: $\sigma_\infty = 1.0$, $\tilde{\sigma} = 0.6$, $\sigma_Q = 0.1$, $\lambda_0 = 0.5$, $s = 100.0$.

Given its heterogeneous structure, it seems reasonable to model the tumour's internal microstructure as a porous medium and to use Darcy's law to describe the motion of the tumour cells through the tissue matrix. Hence, we now introduce the internal pressure p which we assume is related to \mathbf{u} via Darcy's Law [4, 40]

$$\mathbf{u} = -\mu\nabla p,$$

where μ denotes the motility of the tumour cells.

Combining (2.2) and (2.3), we deduce that

$$\mu\nabla^2 p = -S(\sigma, \beta, \omega), \quad (2.4)$$

$$\mathbf{n} \cdot \frac{d\mathbf{r}}{dt} = -\mu\nabla p \cdot \hat{\mathbf{n}} \quad \text{on } \Gamma(\mathbf{r}, t) = 0. \quad (2.5)$$

The following boundary and initial conditions are applied to (2.1), (2.4) and (2.5):

$$0 = \frac{\partial\sigma}{\partial r} = \frac{\partial\beta}{\partial r} = \frac{\partial\omega}{\partial r} = \frac{\partial p}{\partial r} \quad \text{at } \mathbf{r} = 0, \quad (2.6)$$

$$\sigma = \sigma_\infty - 2\alpha\kappa, \beta = \beta_\infty, \omega = 0, p = p_\infty \quad \text{on } \Gamma(\mathbf{r}, t) = 0, \quad (2.7)$$

$$\sigma, \beta, \omega, p, \frac{\partial\sigma}{\partial r}, \frac{\partial\beta}{\partial r}, \frac{\partial\omega}{\partial r}, \frac{\partial p}{\partial r} \quad \text{continuous across } r = R_Q(\theta, \phi, t) \quad \text{and } R_N(\theta, \phi, t), \quad (2.8)$$

$$\sigma = \sigma_Q \quad \text{on } \Gamma_{R_Q}(\mathbf{r}, t) = 0 (\sigma > \sigma_Q \forall \mathbf{r} \Rightarrow R_Q(\theta, \phi, t) = 0), \quad (2.9)$$

$$\sigma = \sigma_N \quad \text{on } \Gamma_{R_N}(\mathbf{r}, t) = 0 (\sigma > \sigma_N \forall \mathbf{r} \Rightarrow R_N(\theta, \phi, t) = 0), \quad (2.10)$$

$$\Gamma(\mathbf{r}, 0) = 0 = r - R(\theta, \phi, 0) \quad \text{prescribed.} \quad (2.11)$$

Equations (2.6) ensure that σ, β, ω and p are bounded at $\mathbf{r} = 0$ whereas (2.7) fixes their values on $\Gamma(\mathbf{r}, t) = 0$. Denoting by $\sigma_\infty, \beta_\infty$ and p_∞ the values of σ, β and p in the outer tissue, we remark that most authors assume continuity of σ, β and p across $\Gamma(\mathbf{r}, t) = 0$ [1] [12, 14, 26, 28, 29, 31, 34]. Here the conditions $\beta = \beta_\infty, p = p_\infty$ are retained but the assumption for σ is relaxed. We assume that σ satisfies the Gibbs–Thomson relation there [35, 36]. With κ denoting the mean curvature, this relation states that on the outer boundary σ is less than σ_∞ by a factor $2\alpha\kappa$, this being the energy needed to maintain the inter-cellular bonds which exist on $\Gamma(\mathbf{r}, t) = 0$. By assuming that the internally-produced inhibitor does not spread outside the tumour, we fix $\omega = 0$ on $\Gamma(\mathbf{r}, t) = 0$. When interior free boundaries exist to separate regions of quiescence, proliferation and necrosis equation (2.8) ensures continuity of σ, β, ω, p and their first derivatives across these boundaries. Equations (2.9) and (2.10) define the free boundaries implicitly. Finally, (2.11) specifies the structure of the tumour boundary at $t = 0$.

Model simplification – radial symmetry

Under conditions of radial symmetry the tumour grows as a sphere of radius $R(t)$, with mean curvature $\kappa = 1/R$. In this case, Eqs. (2.1), (2.4)–(2.5) simplify to give:

$$0 = \frac{1}{r^2} \frac{\partial}{\partial r} \left(r^2 \frac{\partial\sigma}{\partial r} \right) + F_\sigma = \frac{1}{r^2} \frac{\partial}{\partial r} \left(r^2 \frac{\partial\beta}{\partial r} \right) + F_\beta = \frac{1}{r^2} \frac{\partial}{\partial r} \left(r^2 \frac{\partial\omega}{\partial r} \right) + F_\omega, \quad (2.12)$$

$$0 = \frac{\mu}{r^2} \frac{\partial}{\partial r} \left(r^2 \frac{\partial p}{\partial r} \right) + S(\sigma, \beta, \omega), \quad (2.13)$$

$$\frac{dR}{dt} = -\mu \frac{\partial p}{\partial r} \Big|_{r=R(t)}. \quad (2.14)$$

Integrating (2.13) over the tumour volume yields the following expression:

$$\mu R^2 \frac{\partial p}{\partial r} \Big|_{r=R} = \mu \int_0^R \frac{\partial}{\partial r} \left(r^2 \frac{\partial p}{\partial r} \right) dr = - \int_0^R S(\sigma, \beta, \omega) r^2 dr.$$

Substituting in (2.14) we eliminate p from our model, which now comprises (2.12) and

$$R^2 \frac{dR}{dt} = \int_0^R S(\sigma, \beta, \omega) r^2 dr, \quad (2.15)$$

subject to (2.6)–(2.11). In (2.7) $\kappa = 1/R$ and $r = R(t)$ on $\Gamma(\mathbf{r}, t) = 0$. Similarly, $r = R_Q$ on $\Gamma_{R_Q}(\mathbf{r}, t) = 0$ and $r = R_N$ on $\Gamma_{R_N}(\mathbf{r}, t) = 0$.

We remark that (2.15) can be rewritten

$$\frac{d}{dt} \left(\frac{\text{tumour}}{\text{volume}} \right) = \frac{d}{dt} \left(\frac{4}{3} \pi R^3 \right) = \iiint_{\text{tumour}} S(\sigma, \beta, \omega) dV.$$

Thus, (2.15) states that the rate of increase of the tumour volume is equal to the net tumour cell proliferation rate. Many authors have proposed models of this form to describe avascular tumour growth, without referring to either the internal pressure field or the cell velocity. The above analysis shows how such models can arise as special cases of more physically-based models.

Once the interaction terms have been specified, it is possible to determine the evolution of the tumour colony. In the remainder of this paper, we focus on the following simple choices for F_σ , F_β , F_ω and S :

$$F_\sigma = -(\lambda_0 + \lambda_1 \beta) H(r - R_N), \quad F_\beta = -\lambda_2, \quad F_\omega = \lambda_3 H(R_N - r) - \lambda_4, \quad (2.16)$$

$$S = s\sigma H(r - R_Q) - s\tilde{\sigma} H(r - R_N) - s\omega H(R_N - r). \quad (2.17)$$

$$\underbrace{\hspace{1.5cm}}_{\text{(mitosis)}} \quad \underbrace{\hspace{1.5cm}}_{\text{(apoptosis)}} \quad \underbrace{\hspace{1.5cm}}_{\text{(necrosis)}}$$

In (2.16)–(2.17) $H(\cdot)$ denotes the Heaviside step-function ($H(x) = 1$ if $x > 0$, $H(x) = 0$ if $x \leq 0$). The expression for F_σ assumes that σ is consumed by proliferating and quiescent cells at the constant rate λ_0 , and degraded by the externally-supplied inhibitor (β) at the rate $\lambda_1 \beta$. At the same time, β is degraded by the tumour cells at the constant rate λ_2 , and hence we fix $F_\beta = -\lambda_2$. Turning to F_ω , we assume that ω is produced at the constant rate λ_3 by necrotic cells alone and that it decays throughout the tumour volume at the constant rate λ_4 . The proliferation rate (S) comprises three factors: cell production due to mitosis which is restricted to the proliferating region where it occurs at the rate $s\sigma$ (s is a constant of proportionality); cell loss due to apoptosis [6, 7] which is localized in proliferating and quiescent region ($\sigma > \sigma_N$) where it occurs at the constant rate $s\tilde{\sigma}$; and, cell loss due to necrosis which occurs at the rate $s\omega$ when $\sigma < \sigma_N$.

Other choices for the kinetic terms could be employed. The expressions adopted in this paper enable us to focus on describing a methodological approach for studying tumour growth which can be adapted easily to a particular application.

3 Model analysis

By integrating (2.12) it is possible to determine expressions for σ , β and ω in terms of R , R_Q and R_N . When these expressions are substituted into (2.15) the model reduces to an ODE for $R(t)$ coupled to algebraic equations defining F_Q and R_N in terms of R . The exact form of these expressions depends on the tumour's size and structure and the particular blend of nutrients and inhibitors. The resulting models are solved numerically. To complement these results, and to provide insight into how the different physical mechanisms interact, we use asymptotic analysis to focus on two stages of the tumour's development: (i) immediately after the onset of quiescence ($0 < R_Q \ll 1$) and, (ii) when the proliferating region is small ($0 < R - R_Q \ll 1$).

3.1 Uniform growth

When $R_Q = R_N = \beta = \omega = 0$, integration of (2.12) yields the following expression for σ :

$$\sigma = \sigma_\infty = \frac{2\alpha}{R} - \frac{\lambda_0}{6}(R^2 - r^2), \quad (3.1)$$

and (2.15) reduces to

$$\frac{dR}{dt} = -\frac{sR}{3} \left(\frac{\lambda_0 R^2}{15} - (\sigma_\infty - \tilde{\sigma}) + \frac{2\alpha}{R} \right). \quad (3.2)$$

Imposing $\sigma(0, t) > \sigma_Q$ supplies an expression defining the range of R for which the tumour comprises proliferating cells only:

$$\sigma_\infty - \sigma_Q > \frac{\lambda_0 R^2}{6} + \frac{2\alpha}{R}. \quad (3.3)$$

When $\alpha = 0$ (3.3) provides an upper bound on R , with quiescence predicted when $R^2(t) > 6(\sigma_\infty - \sigma)/\lambda_0$. When $\alpha > 0$ there is also a non-zero lower bound for R which we interpret as a nucleation radius: for smaller tumour radii the continuum approach ceases to apply [35, 36].

When $d/dt = 0$ (3.2) shows how the steady state tumour radius depends upon the system parameters. Figures 1(a, b) show how the roots of this equation vary with σ_∞ and α . From Figure 1(b) we note that the existence of steady solutions is confined to a finite range ($0 \leq \alpha \leq \alpha_{max}$), within which there are two steady solutions. It is possible to derive the following expression for α_{max} which could be tested experimentally:

$$\alpha_{max} = \left(\frac{5}{9\lambda_0} \right)^{1/2} (\sigma_\infty - \tilde{\sigma})^{3/2}.$$

Also shown in Figures 1(a, b) are the results of a local stability analysis, obtained by linearizing (3.2) about the steady state solution [7, 29]. This analysis shows that, where it

exists, the steady solution is stable with respect to small, time-dependent perturbations provided the tumour radius is sufficiently large (that is, $R^2 > 5(\sigma_\infty - \tilde{\sigma})/\lambda_0$). In particular, we note that solutions on the upper branch are stable with respect to time-dependent perturbations whereas those on the lower branch are not.

We now outline how the above results are modified in the presence of an externally-supplied inhibitor. In this case β and σ are given by:

$$\beta = \beta_\infty - \frac{\lambda_2}{6}(R^2 - r^2),$$

$$\sigma = \sigma_\infty - \frac{2\alpha}{R} - \frac{\lambda_0}{6}(R^2 - r^2) - \frac{\lambda_1}{6}\left(\beta_\infty - \frac{\lambda_2 R^2}{6}\right)(R^2 - r^2) - \frac{\lambda_1 \lambda_2}{120}(R^4 - r^4),$$

and the ODE governing R can be written

$$\frac{dR}{dt} = -\frac{sR}{3}\left(\frac{\lambda_0 R^2}{15} - (\sigma_\infty - \tilde{\sigma}) + \frac{2\alpha}{R}\right) - \frac{s\lambda_1 R^3}{45}\left(\beta_\infty - \frac{2\lambda_2 R^2}{21}\right). \quad (3.4)$$

Once again, for valid nonquiescent solutions we require $\sigma(0, t) > \sigma_Q$. Using the expressions for σ , β and dR/dt we note that

$$\sigma(0, t)|_{\beta>0} = \sigma(0, t)|_{\beta=0} - \frac{\lambda_1 R^2}{6}\left(\beta(0, t) + \frac{\lambda_2 R^2}{20}\right) < \sigma(0, t)|_{\beta=0},$$

$$\left(\frac{3}{sR} \frac{dR}{dt}\right)_{\beta>0} = \left(\frac{3}{sR} \frac{dR}{dt}\right)_{\beta=0} - \frac{\lambda_1 R^2}{15}\left(\beta(0, t) + \frac{\lambda_2 R^2}{14}\right) < \left(\frac{3}{sR} \frac{dR}{dt}\right)_{\beta=0}.$$

Thus when $\beta > 0$ the minimum nutrient concentration is reduced, quiescence is more rapidly initiated, and the tumour's growth rate diminished. Further insight into the way in which the inhibitor affects the tumour can be gained by focusing on the asymptotic limit $0 < \lambda_1 \ll 1$ which is realized when the rate of nutrient degradation by the inhibitor is weak. We seek steady solutions to (3.4) of the form

$$R \sim R_0 + \lambda_1 R_1,$$

where R_0 is the inhibitor-free ($\beta = 0$) steady state radius and

$$R_1 = -\left(\frac{R_0^4}{2}\right)\left(\frac{\beta_\infty - 2\lambda_2 R_0^2/21}{\lambda_0 R_0^3 - 15\alpha}\right).$$

For valid solutions, $\beta(0) = \beta_\infty - \lambda_2 R_0^2/6 = 0$. Hence

$$\beta_\infty - \frac{2\lambda_2 R_0^2}{21} > \beta(0) > 0,$$

and we deduce that

$$\text{sign}(R_1) = -\text{sign}(R_0^3 - 15\alpha/\lambda_0).$$

Referring to Figure 1(b) we recall that when $\beta = 0$ steady state solutions on the upper branch satisfy $R_0^3 > 15\alpha/\lambda_0$ whereas those on the lower branch satisfy $R_0^3 < 15\alpha/\lambda_0$. Thus we conclude that the inhibitor *reduces* the size of steady solutions on the upper branch and *increases* the size of those on the lower branch.

3.2. Proliferating and quiescent cells

An analysis similar to that presented in §3.1 can be performed to describe other tumour configurations. For example, when the tumour comprises an outer proliferating rim and an inner quiescent region, if $\beta = 0$ then $\sigma(r, t)$ satisfies (3.1) and (2.15) reduces to the following ODE for $R(t)$:

$$\frac{R^2}{s} \frac{dR}{dt} = -\frac{1}{3} \left(\frac{\lambda_0 R^2}{15} - (\sigma_\infty - \tilde{\sigma}) + \frac{2\alpha}{R} \right) (R^3 - R_Q^3) + \frac{\lambda_0 R_Q^3}{30} (R^2 - R_Q^2) - \frac{\tilde{\sigma} R_Q^3}{3}, \quad (3.5)$$

with $R_Q(t)$ defined explicitly in terms of R by imposing $\sigma(R_Q, t) = \sigma_Q$:

$$\sigma_Q = \sigma_\infty - \frac{2\alpha}{R} - \frac{\lambda_0}{6} (R^2 - R_Q^2), \quad (3.6)$$

and $\sigma(0, t) > \sigma_N$ for valid (non-necrotic) solutions.

For more complex tumour structures the resulting equations are rather cumbersome. In such cases it is more instructive to focus on asymptotic limits for which the model equations simplify [22, 30]. We illustrate how this can be achieved by focusing on cases which are of practical interest: immediately after the onset of quiescence ($0 < R_Q \ll 1$); and, when the width of the proliferating rim is small ($0 \leq R - R_Q \ll 1$ with $0 \leq R_N < R_Q$). The final case is frequently observed in the laboratory.

The onset of quiescence

To characterize the size of the quiescent region directly after the onset of quiescence we introduce the small parameter ϵ ($0 < \epsilon \ll 1$) and assume that R and R_Q can be written as follows:

$$R \sim R_0 + \epsilon R_1 + \epsilon^2 R_2 \quad \text{and} \quad R_Q = \epsilon \bar{R}_Q.$$

Substituting into (3.6), the following relationships can be derived when $\beta = 0$:

$$0 = \sigma_\infty - \sigma_Q - \frac{2\alpha}{R_0} - \frac{\lambda_0 R_0^2}{6}, \quad R_1 = 0, \quad \bar{R}_Q^3 = 2R_0 R_2 \left(1 - \frac{6\alpha}{\lambda_0 R_0^3} \right). \quad (3.7)$$

We observe that the variations in $R(t)$ are smaller than those for $R_Q(t)$ ($O(\epsilon^2)$ vs. $O(\epsilon)$). Substituting with (3.7) in (3.5) yields a singular ODE which is regularized by introducing the short timescale $\tau = t/\epsilon^2$:

$$\frac{dR_2}{d\tau} = -\frac{sR_0}{3} \left(\frac{\lambda_0 R_0^2}{15} - (\sigma_\infty - \tilde{\sigma}) + \frac{2\alpha}{R_0} \right), \quad \text{constant.}$$

Thus, in this limit, the tumour radius grows linearly. Our analysis suggests that at the onset of quiescence the quiescent volume expands rapidly whilst the total tumour volume remains approximately constant. It should be possible to validate our predictions by comparison with *in vitro* measurements of R and R_Q [32] (see §5).

The thin proliferating rim

Introducing the small parameter δ ($0 < \delta \ll 1$) we now assume that

$$R \sim \nu_0 + \delta \nu_1, \quad R_Q = \nu_0 + \delta \nu_{Q1} \quad (0 < \delta \ll 1).$$

Substituting into (3.6) we obtain expressions for ν_0 and the width of the proliferating rim:

$$\nu_0 = \frac{2\alpha}{\sigma_\infty - \sigma_Q}, \quad \nu_1 - \nu_{Q1} = \frac{6\alpha \nu_1}{\lambda_0 \psi_0^3}.$$

If $\tilde{\sigma} \sim O(1)$ (*strong apoptosis*) then the timescale $T = \delta t$ is introduced and we deduce from (3.5) that ν_1 satisfies the following ODE:

$$\frac{d\nu_1}{dT} = -\frac{s\tilde{\sigma}}{3} \nu_0.$$

In this case both ν_1 and $\nu_1 - \nu_{Q1}$ decay linearly on a long time-scale ($t \sim O(\delta^{-1})$).

If, however, $\tilde{\sigma} \sim \delta \bar{\sigma}$ (*weak apoptosis*), then in terms of the original timescale

$$\frac{d\nu_1}{dt} = \frac{6s\alpha\sigma_Q \nu_1}{\lambda_0 \nu_0^3} - \frac{s\bar{\sigma}}{3} \nu_0 \equiv \frac{3s\sigma_Q}{4\lambda_0 \alpha^2} (\sigma_\infty - \sigma_Q)^3 \nu_1 - \frac{2s\alpha\bar{\sigma}}{3(\sigma_\infty - \sigma_Q)}.$$

Since $\sigma_\infty > \sigma_Q$, exponential *growth* of ν_1 is predicted on an $O(1)$ -timescale. By comparing these results with *in vitro* measurements of R and R_Q it should be possible to further validate our model (see §5).

3.3 Proliferating, quiescent and necrotic cells

In this case $R_N > 0$ and $\omega \geq 0$. With $\beta = 0$, Eqs. (2.12) and (2.15) eventually lead to the following ODE for $R(t)$:

$$\begin{aligned} \frac{3R^2}{s} \frac{dR}{dt} &= \left\{ \sigma_N - \tilde{\sigma} + \frac{\lambda_0 R^2}{10} - \frac{\lambda_0 R_N^2}{2} + \frac{\lambda_0 R_N^3}{2R} \right\} R^3 \\ &\quad - \left\{ \sigma_N - \tilde{\sigma} + \frac{\lambda_0 R_Q^2}{10} - \frac{\lambda_0 R_N^2}{2} + \frac{\lambda_0 R_N^3}{2R_Q} \right\} R_Q^3 \\ &\quad + \lambda_3 \left(\frac{R_N}{3} - \frac{2R}{5} \right) \frac{R_N^5}{R} + \frac{\lambda_4}{2} \left(\frac{R^2}{3} - \frac{R_N^2}{5} \right) R_N^3. \end{aligned} \quad (3.8)$$

R_Q and R_N are defined implicitly:

$$\sigma_\infty - \frac{2\alpha}{R} = \sigma_N - \frac{\lambda_0 R_N^2}{2} + \frac{\lambda_0 R_N^3}{3R} + \frac{\lambda_0 R^2}{6}, \quad (3.9)$$

$$\sigma_Q = \sigma_N - \frac{\lambda_0 R_N^2}{2} + \frac{\lambda_0 R_N^3}{3R_Q} + \frac{\lambda_0 R_Q^2}{6}. \quad (3.10)$$

Experimental observations of MCS suggest that, given sufficient nutrients, a tumour will evolve towards a configuration in which it is predominantly necrotic. Guided by these

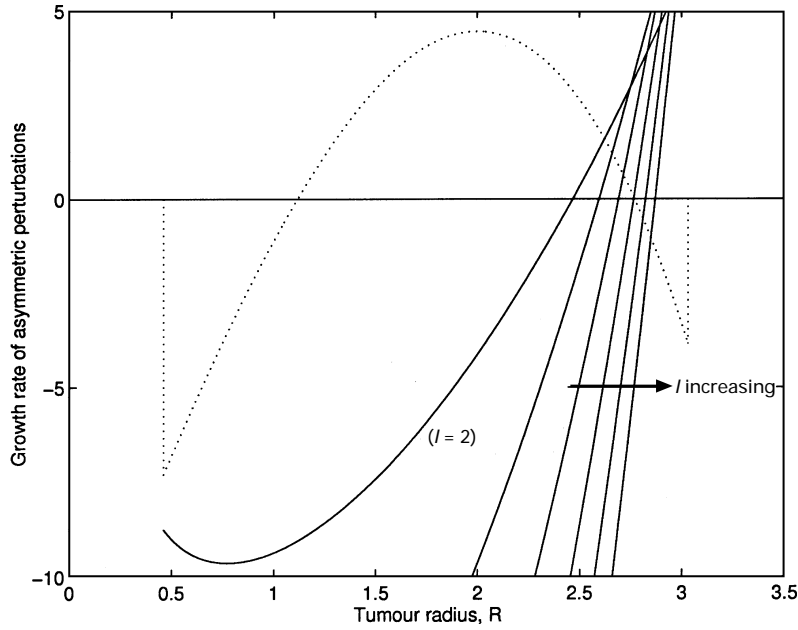


FIGURE 2. Diagram showing how the growth rates of the asymmetric modes $Y_{l,m}(\theta, \phi)$ vary with R . For five choices of l ($l = 2, 3, 4, 5, 6, 7$), $1/\rho_{l,m} d\rho_{l,m}/dt$ is sketched against R . The dotted curve shows how dR/dt varies with R within the feasible range of R . Parameter values: $\sigma_\infty = 1.0$, $\tilde{\sigma} = 0.6$, $\sigma_Q = 0.1$, $\lambda_0 = 0.5$, $\alpha = 0.2$, $s = 100.0$.

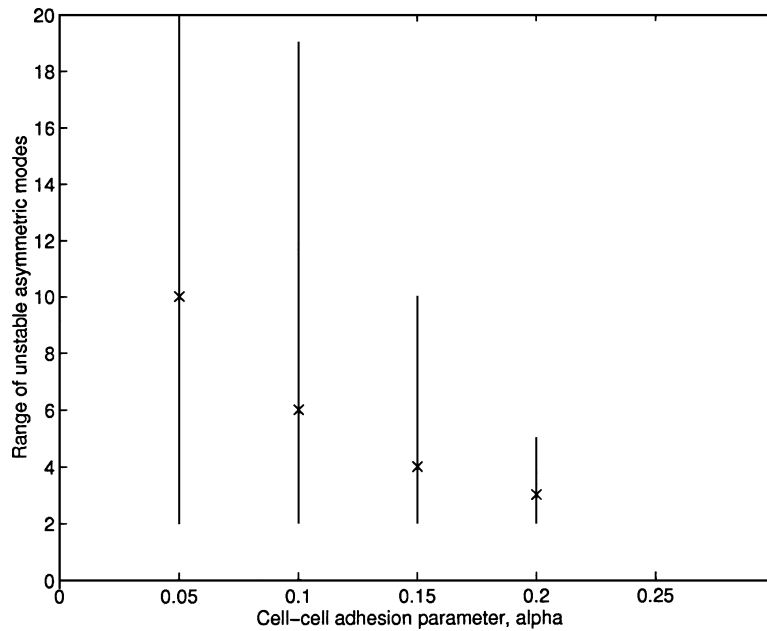


FIGURE 3. Diagram showing those asymmetric modes to which the upper branch of solutions in Figure 1(b) are unstable. As α increases the number of unstable modes and the magnitude of the fastest growing mode fall until for $\alpha > 0.27$ decay of all such asymmetric perturbations from the steady-state is predicted. Parameter values: $\sigma_\infty = 1.0$, $\tilde{\sigma} = 0.6$, $\sigma_Q = 0.1$, $\lambda_0 = 0.5$, $s = 100.0$.

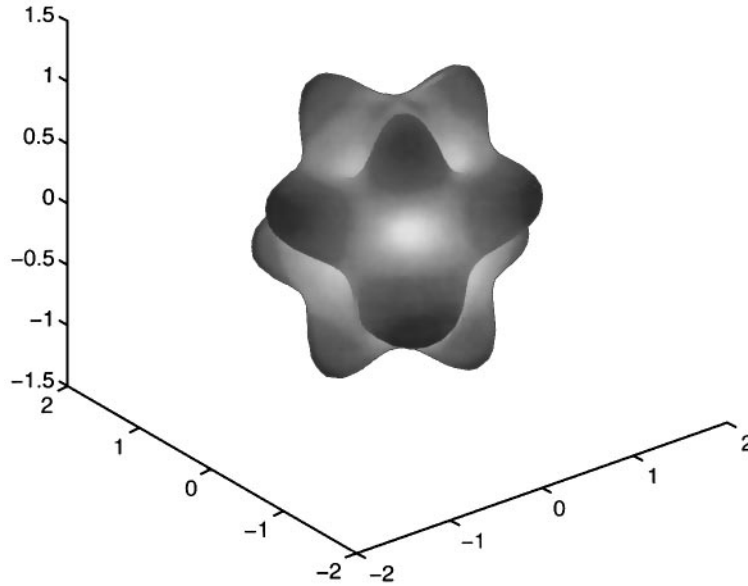


FIGURE 4. Schematic representation of an invading carcinoma for which the mode $Y_{6,3}(\theta, \phi)$ has been excited.

results, and introducing the small parameter η ($0 < \eta \ll 1$), we study equations (3.8)–(3.10) in the limit for which

$$R \sim \hat{R}_0 + \eta \hat{R}_1 + \eta^2 \hat{R}_2, \quad R_Q \sim \hat{R}_0 + \eta \hat{R}_{Q1}, \quad R_N \sim \hat{R}_0 + \eta \hat{R}_{N1}.$$

Substituting into (3.9) and (3.10), we deduce that

$$\begin{aligned} \hat{R}_0 &= \frac{2\alpha}{\sigma_\infty - \sigma_N}, \quad \hat{R}_1 = 0, \\ R_Q - R_N &\sim \eta(\hat{R}_{Q1} - \hat{R}_{N1}) = \sqrt{\frac{2}{\lambda_0}(\sigma_Q - \sigma_N)}, \\ R - R_Q &\sim \eta R_{Q1} = \sqrt{\frac{2}{\lambda_0}(\sigma_Q - \sigma_N)} - \eta \sqrt{\frac{4\alpha \hat{R}_2}{\lambda_0 \hat{R}_0^2}}. \end{aligned}$$

Introducing the timescale $\hat{T} = \eta^2 t$ in (3.8) supplies the following ODE for \hat{R}_2 :

$$\frac{d\hat{R}_2}{d\hat{T}} = \frac{s}{45}(\lambda_4 - \lambda_3) \hat{R}_0^3.$$

The analysis presented above suggests that tumours with thin proliferating rims are only realized if $0 < \sigma_Q - \sigma_N \sim \eta^2 \lambda_0 \ll 1$ and that they evolve to this configuration on a long timescale. Comparison with *in vitro* measurements of R , R_Q and R_N should provide further experimental validation of our model.

4 Asymmetric growth

We now show how asymmetric perturbations from radial symmetry affect the tumour's growth, extending results that pertain to a uniformly proliferating tumour [22]. Here we examine the effect that an external inhibitor has on the stability of the radially symmetric configuration. We also investigate the stability of the radially symmetric tumour when it contains more than one cell type.

4.1 Uniformly proliferating tumour

Following §3.1, we fix $\beta = 0 = R_Q = R_N$ and focus on a uniformly proliferating tumour. Introducing the small parameter ϵ ($0 < \epsilon \ll 1$) we seek solutions to (2.1), (2.4)–(2.11) of the form:

$$\sigma_\epsilon = \sigma(r, t) + \epsilon \bar{\sigma}(r, \theta, \phi, t), \quad p_\epsilon = p(r, t) + \epsilon \bar{p}(r, \theta, \phi, t), \quad R_\epsilon = R(t) + \epsilon \bar{R}(\theta, \phi, t). \quad (4.1)$$

Substituting with (4.1) in (2.1), (2.4)–(2.11) and equating coefficients of $O(1)$ to zero we deduce that the leading order terms satisfy the uniform growth model of §3.1. Thus σ and R satisfy (3.1) and (3.2) and

$$p(r, t) = p_\infty + \frac{s}{6\mu} \left(\sigma_\infty - \bar{\sigma} - \frac{2\alpha}{R} - \frac{\lambda/0 R^2}{6} \right) (R^2 - r^2) + \frac{s\lambda_0}{120\mu} (R^4 - r^4).$$

Equating terms of $O(\epsilon)$ to zero we recover the linearized equations governing $\bar{\sigma}$, \bar{p} and \bar{R} :

$$0 = \nabla^2 \bar{\sigma} = \mu \nabla^2 \bar{p} + s \bar{\sigma}, \quad (4.2)$$

$$\frac{\partial \bar{R}}{\partial t} = -\mu \left(\frac{\partial \bar{p}}{\partial r} + \bar{R} \frac{\partial^2 p}{\partial r^2} \right) \Big|_{r=R(t)}, \quad (4.3)$$

subject to

$$\frac{\partial \bar{\sigma}}{\partial r} = 0 = \frac{\partial \bar{p}}{\partial r} \quad \text{at } r = 0, \quad (4.4)$$

$$\bar{\sigma}(r, \theta, \phi, t) = \frac{\alpha}{R^2} (2\bar{R} + \mathcal{L}(\bar{R})) - \bar{R} \frac{\partial \sigma}{\partial r} \Big|_{r=R(t)}, \quad (4.5)$$

$$\bar{p}(R, \theta, \phi, t) = -\bar{R} \frac{\partial p}{\partial r} \Big|_{r=R(t)}, \quad (4.6)$$

$$\bar{R}(\theta, \phi, 0) = \bar{R}_0(\theta, \phi), \quad \text{prescribed.} \quad (4.7)$$

In (4.5) $\mathcal{L}(\cdot)$ denotes the angular part of the Laplacian operator. We seek separable solutions to (4.2)–(4.7) of the form

$$\bar{\sigma} = \sum \chi_{lm}(t) r^l Y_{lm}(\theta, \phi) \quad \bar{p} = \sum \left\{ \Pi_{lm}(t) - \frac{s\chi_{lm} r^2}{2\mu(2l+3)} \right\} r^l Y_{lm}(\theta, \phi),$$

$$\bar{R} = \sum \rho_{lm}(t) Y_{lm}(\theta, \phi),$$

where the spherical harmonics $Y_{lm}(\theta, \phi)$ satisfy $\nabla^2(r^l Y_{lm}) = 0$ and $\bar{\sigma}$ and \bar{p} automatically

satisfy (4.2) and (4.4). Imposing (4.5) and (4.6) yields expressions defining χ_{lm} and Π_{lm} which when combined with (4.3) lead to the following ODE for ρ_{lm} :

$$\frac{1}{s\rho_{lm}} \frac{d\rho_{lm}}{dt} = -\frac{(l-1)}{3} \left\{ \sigma_\infty - \tilde{\sigma} - \left(\frac{l}{2l+3} \right) \frac{\alpha}{R} - \left(\frac{2l+9}{2l+3} \right) \frac{\lambda_0 R^2}{15} \right\}, \quad (4.8)$$

We remark that $d\rho_{lm}/dt = 0$ when $l = 1$. This arises because the mode for which $l = 1$ represents a translation of the axes. It is also consistent with other results [24, 35, 41, 42]. We remark further that the evolution of ρ_{lm} is independent of the azimuthal component m .

Since $R(t)$ is a dynamic variable, a particular mode Y_{lm} may be excited for one range of R and damped for another. This situation is depicted in Figure 2, where the right-hand side of (4.8) is sketched for several choices of l . The dashed curve shows how dR/dt varies with R over the range defined by (3.3) and points to the existence of a radially-symmetric solution which is stable with respect to time-dependent perturbations. The continuous curves suggest that this steady state is unstable with respect to a finite range of asymmetric perturbations ($2 \leq l \leq 5$).

When $dR/dt = 0$ (4.8) reduces to give

$$\frac{1}{s\rho_{lm}} \frac{d\rho_{lm}}{dt} = \frac{(l-1)}{2l+3} \left\{ \frac{2\lambda_0 R^2}{15} - (l+2) \frac{\alpha}{R} \right\}, \quad (4.9)$$

and we conclude that when $\alpha = 0$ the radially-symmetric steady-state solution is *unstable* with respect to all modes Y_{lm} for which $l \geq 2$. More generally ($\alpha > 0$), we deduce that the steady-state is stable to modes for which $l+2 > 2\lambda_0 R^3/15\alpha$. Thus, for a given value of R , only a finite number of modes are excited, the choice of parameter values defining both the size of the steady state radius R and the unstable range of l . This result also demonstrates the stabilizing effect that cell-cell adhesion has on the tumour's growth: as α increases the range of l to which the steady state is unstable decreases.

Differentiating (4.8) with respect to l we can determine the fastest growing mode for a given value of $R(t)$. After some simple analysis we deduce that the fastest growing mode satisfies the following quadratic equation:

$$0 = (2l^2 + 6l - 3) \frac{\alpha}{R} + (4l^2 + 12l + 39) \frac{\lambda_0 R^2}{15} - (2l+3)^2 (\sigma_\infty - \tilde{\sigma}). \quad (4.10)$$

In Figure 3 we focus on the stability of the upper branch of steady solutions presented in Figure 1. As α varies we plot the range of l to which the relevant steady state is unstable. The fastest growing mode is also marked. From the diagram we note that as α increases the steady state radius decreases and the range of instability decreases until, for α sufficiently large ($\alpha > 0.27$), the steady state is stable with respect to all asymmetric modes.

Figure 4 shows how the size and shape of a radially-symmetric tumour alters when it is subjected to an asymmetric disturbance. At a given time, the mode which dominates the instability is selected from (4.10). As $R(t)$ evolves the order of the dominant mode changes. Referring to Greenspan [24], we remark that if the instability which develops is controlled by nonlinear processes, not included in the present model, the tumour may reach a new equilibrium. Otherwise, it may split into smaller tumours. These secondary tumours (or metastases) might eventually also split, continuing the growth and invasion of the cancer.

This analysis may provide a description of the initiation of the irregular morphology which characterizes the growth of carcinomas. As such it may be viewed as describing the transition or bifurcation from the radially symmetric configurations studied by Adam and others [26–31] to the highly irregular or fractal structure studied by Cross and others [43–45].

We can repeat the above analysis with $\beta > 0$ to derive the analogue of (4.8) which describes the evolution of the asymmetric perturbations in the presence of an externally-supplied inhibitor:

$$\frac{1}{s\rho_{lm}} \frac{d\rho_{lm}}{dt} = -\frac{(l-1)}{3} \left\{ (\sigma_\infty - \tilde{\sigma}) - \frac{l}{2l+3} \frac{\alpha}{R} - \frac{(2l+9)}{(2l+3)} \lambda_0 R^2 \right\} \\ - \frac{\lambda_1 \lambda_2 R^4}{3(2l+3)} \left\{ \frac{(l-1)\beta_\infty}{\lambda_2 R^2} + \frac{1}{15} + \frac{1}{(2l+3)(2l+5)} - \frac{2(l+2)(2l+3)}{15 \cdot 21} \right\}. \quad (4.11)$$

As expected, $d\rho_{lm}/dt = 0$ when $l = 1$. The second term on the right-hand-side of (4.11) shows how the inhibitor affects the growth rate of the modes. If β_∞/λ_2 is sufficiently large then for moderate values of l this term will be positive and we infer that the inhibitor destabilises the growth rate of such modes. Ultimately, (for large l) the stabilizing quadratic term dominates so that, as when $\beta = 0$, the range of l for which asymmetric growth occurs is finite.

4.2 Proliferating and quiescent cells

Similar analysis enables us to extend results that describe the stability of tumours with thin proliferating rims [24] to cases for which the width of the proliferating rim is arbitrary. In this case, at leading order we recover the radially-symmetric model of §3.2 for which $R(t)$ and $R_Q(t)$ satisfy eqs. (3.5) and (3.6). With $\Phi_Q(t) = R_Q/R \in [0, 1)$, and continuing to $O(\epsilon)$ it is possible to show that in the absence of any inhibitors the coefficients ρ_{lm} satisfy the following ODEs:

$$\frac{1}{s\rho_{lm}} \frac{d\rho_{lm}}{dt} = -\frac{(l-1)}{3} \left\{ \sigma_\infty - \tilde{\sigma} - \frac{2\alpha}{R} - \frac{(2l+9)}{(2l+3)} \frac{\lambda_0 R^2}{15} \right\} \\ - \frac{\alpha}{R} (l-1)(l+2) \left\{ \frac{1 - \Phi_Q^{2l+2}}{2l+3} + \frac{3\sigma_Q}{\lambda_0 P^2} \Phi_Q^{2l} \right\} + \left(\sigma_Q - \frac{\lambda_0 R_Q^2}{15} \right).$$

In particular, when $l = 1$ we have

$$\frac{1}{s\rho_{1m}} \frac{d\rho_{1m}}{dt} = -\Phi_Q^2 (1 - \Phi_Q) \left(\sigma_Q - \frac{\lambda_0 R_Q^2}{15} \right).$$

Using (3.6) we have

$$\sigma_Q - \frac{\lambda_0 R_Q^2}{15} = \sigma(0, t) + \frac{\lambda_0 R_Q^2}{10} > 0.$$

Using this result and noting that $\Phi_Q \in [0, 1)$, we deduce that $1/s\rho_{1m} d\rho_{1m}/dt \leq 0$, with equality in the limits $\Phi_Q \rightarrow 0, 1$, i.e. as the quiescent region disappears or as the width of the proliferating rim shrinks to zero. These results are consistent with the analysis of §4.1 ($\Phi_Q = 0$) and with Greenspan's results [24] ($\Phi_Q \rightarrow 1$). The results for intermediate values of Φ_Q

are new and suggest that the quiescent cell population stabilizes the radial structure of the tumour. Once again comparison with *in vitro* data should enable us to validate our model predictions (see §5).

4.3 Proliferating and necrotic cells

By assuming that $\sigma_N > \sigma_Q$, it is possible to study cases for which $R_N > R_Q = 0$. The radially-symmetric model is recovered at leading order. Introducing $\Phi_N = R_N/R$ it is possible to show that the equilibrium tumour radii R and R_N (or Φ_N) satisfy

$$\sigma_\infty - \tilde{\sigma} - \frac{2\alpha}{R} = \frac{\Gamma R^2}{6} (1 - \Phi_N)^2 (1 + 2\Phi_N), \quad (4.12)$$

$$\lambda \Phi_N^3 = (\sigma_N - \tilde{\sigma})(1 - \Phi_N^3) - \frac{\Gamma R^2}{2} \Phi_N^2 (1 - \Phi_N) + \frac{\Gamma R^2}{10} (1 - \Phi_N^5). \quad (4.13)$$

Continuing to $O(\epsilon)$ yields an equation which describes the evolution of the amplitudes of the asymmetric perturbations to the radially-symmetric configuration:

$$\frac{1}{s\rho_{lm}} \frac{d\rho_{lm}}{dt} = \sigma_\infty - \tilde{\sigma} - \frac{2\alpha}{R} - \frac{A}{2l+3} - A\Phi_N^{2l} \left(\frac{2l\Phi_N^2}{3(2l+3)} + \frac{1}{3} + \frac{2l}{\Gamma R^2} (\sigma_N - \tilde{\sigma} + \lambda) \right), \quad (4.14)$$

where

$$A = \frac{1}{1 - \Phi_N^{2l}} \left(\frac{\alpha}{R} (l+2)(l-1) + \frac{\alpha R^2}{3} (1 - \Phi_N^3) \right).$$

The influence of the various physical mechanisms is somewhat obscured in this equation. However, by focusing on limiting cases some insight can be obtained. For example, if the necrotic core is very small ($0 < \Phi_N \ll 1$) then (4.14) reduces to (4.8). The limit $0 < 1 - \Phi_N \ll 1$ describes a predominantly necrotic tumour, a structure frequently observed when MCS are grown *in vitro*. Taking the limit $\Phi_N \rightarrow 1$ in (4.12) and (4.13) we deduce that a necessary condition for obtaining steady solutions with thin proliferating rims is that the rate of necrotic cell loss be such that

$$\lambda \sim O(1 - \Phi_N).$$

In this case the steady state tumour radius satisfies

$$\sigma_\infty - \tilde{\sigma} - \frac{2\alpha}{R} \sim O(1 - \Phi_N)^2,$$

and the amplitudes of the asymmetric modes satisfy

$$\frac{1}{s\rho_{lm}} \frac{d\rho_{lm}}{dt} \sim -\frac{2\alpha(l+2)(l-1)}{R(1 - \Phi_N^{2l})} \left(\frac{1}{3} + \frac{l(\sigma_N - \tilde{\sigma})}{\Gamma R^2} \right).$$

Once again, the system is stable with respect to the first spherical harmonic ($l = 1$). It is also stable with respect to all higher order spherical harmonics ($l > 1$). This differs from the analysis presented in §4.2 because we assume that the necrotic core is a stabilizing *sink* of tumour cells. The analysis presented above suggests that the stability, with respect to asymmetric perturbations, of MCS depends crucially on their structure, for example whether they possess a necrotic core. It should be possible to test such predictions experimentally by observing the response of various MCS whose outer boundaries have been deformed.

5 Conclusions

In this paper we have presented a model for the growth of an avascular tumour or multicellular spheroid, which has extended previous work on this subject. The modelling has incorporated important physical quantities such as internal tumour pressure and cell-cell adhesion which are experimentally measurable [20, 21, 32]. Coupled with explicit tracking of the tumour radius this puts our model on a firm foundation, leading potentially to *quantitative* analysis. Previous models have favoured a more qualitative viewpoint. Our model formulation has led naturally to the incorporation of free boundaries which define the outer tumour surface and various inner surfaces, such as the boundary of the necrotic core or the quiescent region. The model faithfully reproduces many of the features associated with avascular solid tumour growth such as evolution to a stable, structured steady state. The analysis also reveals that the structure depends crucially on nutrient supply. A time-dependent asymptotic analysis reveals that there is initial rapid growth of the quiescent and necrotic regions when they first appear in the tumour. This is in good agreement with independent experimental observations [32].

Similar analysis leads us to predict that if the rate of cell loss due to apoptosis ($\tilde{\sigma}$) is comparable with the external nutrient concentration (σ_∞) then the tumour will evolve, on a long timescale, to a steady configuration wherein the tumour possesses a thin proliferating rim – a configuration frequently observed when MCS are grown *in vitro* [8, 9, 32, 46]. It should be possible to perform experiments that verify whether these physical conditions hold for MCS with this proliferating rims.

The linear stability analysis (i.e. asymmetric spatial perturbations) reveals that the stability of the growing MCS depends on certain key parameters of the model; namely, strength of adhesion bonds and external nutrient concentration. This analysis may provide a description of the initiation of the irregular morphology which characterises the growth of carcinomas. As such, it offers a possible explanation of the bifurcation from the radially-symmetric growth studied by Adam and others [26, 27, 29, 31] to the fractal structure studied by Cross and others [43, 45].

In summary, the model provides a general framework to describe the growth of MCS, reproduces experimental observations and, perhaps most importantly, makes predictions which are experimentally verifiable (cf. [20, 21, 32, 46, 47]).

References

- [1] CHADAM, J., HOWISON, S. D. & ORTALEVA, P. (1987) Existence and stability for spheroidal crystals growing in a supersaturated solution. *IMA J. Appl. Math.* **39**, 1–15.
- [2] CHADAM, J. M. & RASMUSSEN, H. (1993) *Emerging Applications in Free Boundary Problems*. Longman Group.
- [3] CRANK, J. (1988) *Free and Moving Boundary Problems*. Oxford University Press.
- [4] ELLIOTT, C. & OCKENDON, J. R. (1982) Weak and variational methods for moving boundary problems. *Research Notes in Mathematics* 59. Pitman, London.
- [5] MURRAY, J. D. (1990) *Mathematical Biology*. Springer-Verlag, Berlin, Germany.
- [6] KERR, J. F. R. (1971) Shrinkage necrosis; a distinct mode of cellular death. *J. Path.* **105**, 13–20.
- [7] KERR, J. F. R., WYLLIE, A. H. & CURRIE, A. R. (1972) Apoptosis: a basic biological phenomenon with wide-ranging implications in tissue kinetics. *Br. J. Cancer* **26**, 239–257.

- [8] SUTHERLAND, R. M. & DURAND, R. E. (1984) Growth and cellular characteristics of multicell spheroids. *Recent Results in Cancer Research* **95**, 24–49.
- [9] SUTHERLAND, R. M. (1988) Cell and environment interactions in tumor microregions: the multicell spheroid model. *Science* **240**, 177–184.
- [10] TUBIANA, M. (1971) The kinetics of tumour cell proliferation and radiotherapy. *Br. J. Radiol.* **44**, 325–347.
- [11] BALDING, D. & McELWAIN, D. L. S. (1985) A mathematical model of tumour-induced capillary growth. *J. Theor. Biol.* **114**, 53–73.
- [12] BYRNE, H. M. & CHAPLAIN, M. A. J. (1995) Mathematical models for tumour angiogenesis: numerical simulations and nonlinear wave solutions. *Bull. Math. Biol.* **57**, 461–486.
- [13] CHAPLAIN, M. A. J. & STUART, A. M. (1993) A model mechanism for the chemotactic response of endothelial cells to tumour angiogenesis factor. *IMA J. Math. Appl. Med. Biol.* **10**, 149–168.
- [14] CHAPLAIN, M. A. J. & BRITTON, N. F. (1993) On the concentration profile of a growth inhibitory factor in multicell spheroids. *Math. Biosci.* **115**, 233–245.
- [15] ORME, M. E. & CHAPLAIN, M. A. J. (1996) A mathematical-model of the first steps of tumour-related angiogenesis – capillary sprout formation and secondary branching. *IMA J. Math. Appl. Med. Biol.* **13**, 73–98.
- [16] STOKES, C. L. & LAUFFENBURGER, D. A. (1991) Analysis of the roles of microvessel endothelial cell random motility and chemotaxis in angiogenesis. *J. Theor. Biol.* **152**, 377–403.
- [17] FOLKMAN, J. (1974) Tumour angiogenesis. *Adv. Cancer Res.* **19**, 331–358.
- [18] FOLKMAN, J. (1976) The vascularisation of tumours. In: E. C. Friedberg (ed.), *Cancer Biology*. Scientific American, pp. 115–124.
- [19] MUTHUKARRUPAN, V. R., KUBAI, L. & AUERBACH, R. (1982) Tumour-induced neovascularisation in the mouse eye. *J. Natl. Cancer Inst.* **69**, 699–705.
- [20] JAIN, R. K. (1993) Physiological resistance to the treatment of solid tumours. In: B. A. Teicher (ed.), *Drug Resistance in Oncology*. Marcel Dekker.
- [21] JAIN, R. K. (1994) Barriers to drug delivery in solid tumours. *Scientific American* **271** (1), 58–65.
- [22] BYRNE, H. M. & CHAPLAIN, M. A. J. (1996) Modelling the role of cell-cell adhesion in the growth and development of carcinomas. *Math. Comput. Modelling* **24**, 1–17.
- [23] CHAPLAIN, M. A. J. (1993) The development of a spatial pattern in a model for cancer growth. In: Othmer, H. G., Maini, P. K. & Murray, J. D. (eds.), *Experimental and Theoretical Advances in Biological Pattern Formation*, pp. 45–60. Plenum Press.
- [24] GREENSPAN, H. P. (1976) On the growth and stability of cell cultures and solid tumours. *J. Theor. Biol.* **56**, 229–242.
- [25] ORME, M. E. & CHAPLAIN, M. A. J. (1996) A mathematical-model of vascular tumour-growth and invasion. *Math. Comput. Modelling* **23**, 43–60.
- [26] ADAM, J. A. (1987) A mathematical model of tumour growth. II. Effects of geometry and spatial uniformity on stability. *Math. Biosci.* **86**, 183–211.
- [27] ADAM, J. A. (1987) A mathematical model of tumor growth. III: Comparison with experiment. *Mat. Biosci.* **86**, 213–227.
- [28] ADAM, J. A. & MAGGELAKIS, S. A. (1990) Diffusion regulated growth characteristics of a spherical prevascular carcinoma. *Bull. M. Bio.* **52**, 549–582.
- [29] BYRNE, H. M. & CHAPLAIN, M. A. J. (1995) Growth of non-necrotic tumours in the presence and absence of inhibitors. *Math. Biosci.* **130**, 151–181.
- [30] BYRNE, H. M. & CHAPLAIN, M. A. J. (1996) Growth of necrotic tumours in the presence and absence of inhibitors. *Math. Biosci.* **135**, 187–216.
- [31] GREENSPAN, H. P. (1972) Models for the growth of a solid tumour by diffusion. *Stud. Appl. Math.* **52**, 317–340.
- [32] GROEBE, K. & MUELLER-KLIESER, W. (1996) On the relation between size of necrosis and diameter of tumour spheroids. *Int. J. Rad. Onc. Biol. and Phys.* **34**, 395–401.

- [33] MCELWAIN, D. L. S. & MORRIS, L. E. (1978) Apoptosis as a volume loss mechanism in mathematical models of solid tumour growth. *Math. Biosci.* **39**, 147–157.
- [34] MAGGELAKIS, S. A. & ADAM, J. A. (1990) Mathematical model of prevascular growth of a spherical carcinoma. *Math. Comput. Modelling* **13**, 23–38.
- [35] LANGER, J. S. (1980) Instabilities and pattern formation in crystal growth. *Rev. Mod. Phys.* **52**, 1–20.
- [36] MULLINS, W. W. & SEKERKA, R. F. (1963) Morphological stability of a particle growing by diffusion or heat flow. *J. Appl. Phys.* **34**, 323–329.
- [37] MIYASAKA, M. (1995) Cancer metastasis and adhesion molecules. *Clin. Orth. Rel. Res.* **312**, 10–18.
- [38] NAGLE, R. B., KNOX, J. D., WOLF, C., BOWDEN, G. T. & CRESS, A. E. (1994) Adhesion molecules, extracellular matrix and proteases in prostate carcinoma. *J. Cell. Biochem.* **19S**, 232–237.
- [39] FOLKMAN, J. & HOCHBERG, M. (1973) Self-regulation of growth in three dimensions. *J. Exp. Med.* **138**, 745–753.
- [40] NEWMANN, S. P. (1977) Theoretical derivation of Darcy's Law. *Acta Mechan.* **25**, 153–170.
- [41] SCHWEGLER, H., TARUMI, K. & GERSTMANN, B. (1985) Physico-chemical model of a protocell. *J. Math. Biol.* **22**, 335–348.
- [42] SCHWEGLER, H. & TARUMI, K. (1986) The 'protocell': a mathematical model of self-maintenance. *BioSystems* **19**, 307–315.
- [43] CROSS, S. S. & COTTON, D. W. K. (1992) The fractal dimension may be a useful morphometric discriminant in histopathology. *J. Pathol.* **166**, 409–411.
- [44] CROSS, S. S., BURY, J. P., SILCOCKS, P. B., STEPHENSON, T. J. & COTTON, D. W. K. (1994) Fractal geometric analysis of colorectal polyps. *J. Pathol.* **172**, 317–323.
- [45] LANDINI, G. & RIPPIN, J. W. (1996) How important is tumour shape? *J. Pathol.* **179**, 210–217.
- [46] MUELLER-KLIESER, W. (1995) Metabolic milieu – a response modifier in multicell spheroids. *Proceedings of the Tenth International Congress of Radiation Research*, vol. 2, pp. 827–830.
- [47] GROEBE, K. & MUELLER-KLIESER, W. (1991) Distributions of oxygen, nutrient and metabolic waste concentrations in multicellular spheroids and their dependence on spheroid parameters. *Euro. Biophys. J.* **19**, 169–181.